Models for Induction Machines with Magnetic Saturation of the Main Flux Path

Charles R. Sullivan, *Student Member, IEEE*, and Seth R. Sanders, *Member, IEEE*

Abstract—**A new nonlinear π model for an induction machine operating in magnetic saturation has been developed. It is based on a magnetic circuit model of a rotor-stator tooth pair, with nonlinear reluctance elements representing the saturation in the rotor and in the stator. The model of a tooth pair is extended to a model of the machine by assuming an infinite number of infinitesimal teeth. The model is compatible with the Blondel-Park transformation. Experimental measurements on a wound-rotor machine validate the new model. Operating conditions for optimal efficiency at high torque levels requiring operation in saturation are computed.**

I. Introduction

INDUCTION machines are usually modeled with the assumption of linear magnetics. However, in many variable-torque applications, it is desirable to operate in saturation, allowing an induction machine to produce higher torque. For example, in vehicular applications, the induction machine may be sized for normal road conditions. However, to overcome extreme inclines or to permit high acceleration or deceleration rates, it is necessary to produce high instantaneous torque. Thus, a smaller machine may be used if its control system can maintain control through peak torque demand. Traditionally, inductance values used for control or calculations are adjusted to compensate for saturation effects. However, this is not always adequate. More precise modeling of saturation becomes essential for control purposes and for understanding the limitations imposed by saturation.

It has been recently noted that saturation effects in smooth air-gap machines can introduce cross-coupling effects that are not predicted by linear models. In a two-axis machine (or model) the current in one winding can affect the flux in the orthogonal winding. The "cross saturation" model [1]–[8] has become the standard method of accounting for these effects. The model is based on the conventional T model of an induction motor, and the saturation is assumed to be entirely in the mutual inductance, not in the leakage, as shown in Fig. 1. While the T model with saturating mutual inductance gives reasonable accuracy in simulations, it can be inconvenient to use when the machine is connected to a voltage source, since it is most naturally a current-controlled rather than a flux-controlled model. In [4], for example, the T model is transformed to a π model for the purposes of simulation.

Because the form of the T model with saturating mutual inductance is merely postulated by extending a standard linear model to include saturation of the mutual path, our work develops a new model, based on a nonlinear magnetic circuit model of the machine. The resulting model is in fact most naturally a π model, and so we avoid the need to transform it for simulations or control designs. In the linear-magnetics case, a π model is equivalent to a T model. With saturation, however, the two are no longer equivalent. Although the π model can provide a more accurate model for the saturated induction machine, of greater importance, the π form is more convenient for field-oriented control designs that take magnetic saturation into account [9], [10].

Essential to much conventional analysis and control is the ability to perform a Blondel-Park transformation, as discussed for the general linear-magnetics case in [11]. The T model is shown in [5] to allow the transformation. The new π model is also shown to allow the transformation. An analysis of torque production, taking care to account for nonlinear effects, shows that several familiar expressions for torque are still correct with a saturated machine.

We have used several different experimental methods to determine the characteristics of a wound rotor machine and compare them to the model. Blocked rotor tests with the rotor and stator fed from separate voltage sources serve to verify the magnetic model. Steady-state shorted-rotor operation tests on the same machine with torque measurements and electrical measurements only from stator terminals serve to verify the torque predictions of the model, and also verify that it is possible to characterize the π model saturation characteristics without access to the rotor terminals.

In a further section, steady-state operation in saturation is considered. Specifically, optimal efficiency excitation is discussed, and numerically computed.

II. Magnetic Circuit Models

To derive the appropriate form for a model of an induction machine in magnetic saturation, we use standard magnetic circuit modeling, augmented by the use of nonlinear reluctances to represent saturating portions of the steel. The B-H characteristic of the steel is assumed to be a single-valued nonlinear monotonic function, generally having a shape such as the curve in Fig. 2. The flux/MMF characteristic of the reluctance element, for simple geometries, is just the B-H characteristic, scaled by cross-sectional area for flux, and by

Paper IPCSD 95–11, approved by the Electric Machines Committee of the IEEE Industry Applications Society for presentation at the 1992 IEEE Industry Applications Society Annual Meeting, Houston, TX, October 4–9. This work received support from an NSF Graduate Fellowship and by NSF Grant ECS-9358284. Manuscript released for publication January 20, 1995.

The authors are with the Electrical Engineering and Computer Sciences Department, University of California, Berkeley, CA 94720 USA.

IEEE Log Number 9411108.

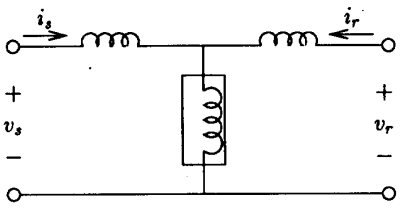

Fig. 1. Nonlinear T model of one phase of a saturating induction machine, with rotor and stator mechanically aligned. Boxed element is nonlinear.

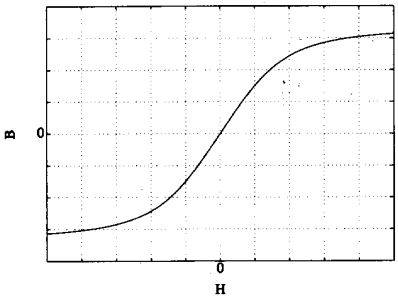

Fig. 2. Typical saturation characteristic.

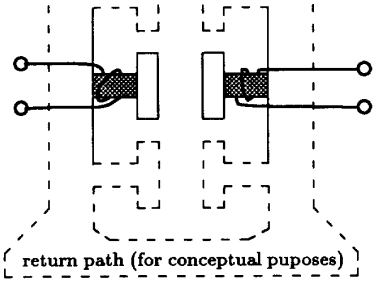

Fig. 3. Simplified tooth structure.

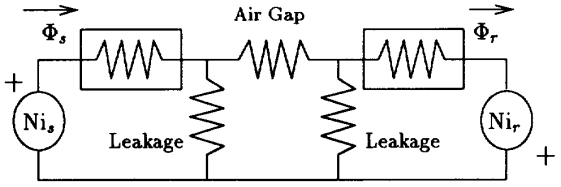

Fig. 4. Magnetic circuit of tooth pair. Boxed elements are nonlinear.

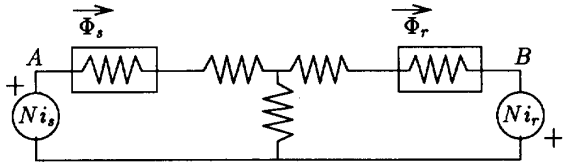

Fig. 5. Modified magnetic circuit of a tooth pair with the center π circuit replaced by a T circuit.

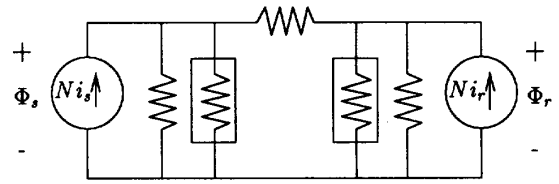

Fig. 6. The dual of the modified magnetic circuit.

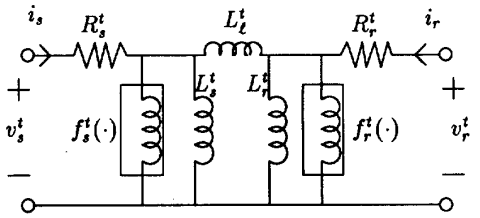

Fig. 7. Electric circuit of tooth pair.

length for MMF. Useful characteristics of this function are that it is invertible, symmetric, and monotonic. We will represent it by $NI = f(\Phi)$, or $\Phi = (f)^{-1}(NI)$, where Φ is the flux and NI is the MMF.

Fig. 3 shows the simplified tooth structure for a single pair of teeth in an induction machine. Fig. 4 shows one way of drawing a magnetic circuit model for the tooth pair, making the assumption that the only portions of the steel that saturate are the central legs, shown shaded in Fig. 3. Especially in a multi-pole (four or more poles) machine, this is a good assumption, because the flux-carrying requirements for the yoke are relatively low. In a two-pole machine, however, the yoke may also saturate if its cross section is not large enough. Thus, this model is valid for most multi-pole machines, but may not work as well for some two-pole machines.

We proceed with a series of transformations to get to an electrical circuit model. Since the central section of the circuit in Fig. 4 is a linear π circuit, it can be replaced by an equivalent T circuit, as shown in Fig. 5. Next, we take the dual of the circuit in Fig. 5 to get the circuit in Fig. 6, with flux as the across variable and MMF as the through variable. Scaling by the number of turns[1] we can reformulate the circuit in terms of flux linkages and current. The circuit is then of exactly the same form as Fig. 6, but has scaled elements. The last step in getting an electric circuit is to convert from flux linkage to voltage by differentiating with respect to time. The resistive elements get replaced by inductances, and the final model for the tooth pair, shown in Fig. 7, results. Fig. 7 also includes resistors, R_s^t and R_r^t, representing the electrical resistance of the stator and rotor windings, with the superscript t used to indicate quantities associated with a single tooth.

As a result of the transformation of the π circuit to a T circuit in moving from Figs. 4 and 5, the linear inductors in Fig. 7 no longer correspond directly to physical parts of the machine. However, the nonlinear inductors correspond directly to the nonlinear reluctance in the shaded portion of the tooth in Fig. 3. For convenience and clarity, we lump the linear portion of the nonlinear inductors with the parallel linear inductors, L_s^t and L_r^t.

[1] We assume for simplicity that the numbers of turns on the rotor and stator are equal. Unequal numbers of turns can be treated by the appropriate scaling.

As drawn, the circuit in Fig. 7 could have circulating currents in various loops of inductors. In the linear case these correspond to unobservable, uncontrollable modes that are of no consequence. In the nonlinear case, the circulating current would not appear directly at the rotor and stator terminals, yet could affect the apparent nonlinear characteristics of the inductances. There are, however, additional constraints resulting from the magnetic circuit. From Fig. 5, the analogy to Kirchhoff's current law requires that the flux through the two stator reluctances be equal, that the flux through the two rotor reluctances be equal, and that the flux through the leakage path be equal to the difference in the rotor and stator fluxes. In Fig. 7, these become the constraints that the flux linkage in L_ℓ^t must be equal to the difference in flux linkages in L_r^t and L_s^t, the flux linkages in $f_s^t(\cdot)$ and L_s^t must be equal, and the flux linkages in $f_r^t(\cdot)$ and L_r^t must be equal. Note that these constraints would be satisfied automatically by the circuit of Fig. 7, given initial conditions with zero circulating current, but adding the algebraic constraint is advantageous because it reduces the order of the model.

III. Vector Characteristics of Saturation

To move from the model of a single tooth pair to a model of a symmetric induction machine, we first step back and consider the vector characteristics of a simpler structure, a machine with windings only on the stator. The model of each tooth can then just be a single nonlinear reluctance, described by $f^t(\Phi) = NI$, where $f^t(\cdot)$ now includes the linear part of the reluctance. To model this machine, we consider the stator to be constructed of an infinite number of infinitesimal teeth, each with the appropriate number of turns of each phase, according to the sinusoidal winding distribution. For simplicity, we consider a two-axis model, but note that the standard transformations may be used to model a three-phase machine. To determine the flux linkage in the windings due to a current in one winding, we integrate

$$\vec{\lambda} = \begin{bmatrix} \lambda_d \\ \lambda_q \end{bmatrix} = F^{-1}(\vec{\imath}) = \begin{bmatrix} \displaystyle\int_0^{2\pi} N\cos\,\theta (f^t)^{-1}(Ni_d\cos\,\theta + Ni_q\sin\,\theta)\,d\theta \\ \displaystyle\int_0^{2\pi} N\sin\,\theta (f^t)^{-1}(Ni_d\cos\,\theta + Ni_q\sin\,\theta)\,d\theta \end{bmatrix}. \tag{1}$$

For a given numerical or analytic form of $(f^t)^{-1}(\cdot)$, this could be solved explicitly. However, in a typical practical situation, $(f^t)^{-1}(\cdot)$ is not known, and is not easy to measure. The function $F(\cdot)$ describes the overall terminal quantities, and so is easier to measure. However, even without measuring either function, we can deduce some characteristics of the function $F(\cdot)$ from the form of (1).

In (1) we are taking the result of applying a nonlinear function $(f^t)^{-1}(\cdot)$ to a sinusoid, and extracting the component at the fundamental frequency of the input. This situation has been analyzed extensively in nonlinear control system theory, where it is called *describing function* analysis [12]. Describing function analysis is generally applied to sinusoidal functions of time, but we can apply it just as well to a sinusoidal function of spatial angle in the machine. Describing function analysis is generally an approximate method, because the assumption that the input is a sine wave is usually not exact, and because ignoring all harmonics at the output may also involve some approximation. However, for the analysis of the hypothetical machine with only stator windings and an infinite number of teeth, the method is exact. The input is forced to be a sinusoid by the sinusoidal winding pattern, and the output harmonics are of no consequence, because only the fundamental component contributes to the flux linkage in the sinusoidal windings.

With describing function analysis of functions of time, it can be shown that a memoryless nonlinearity produces no phase shift between the input and output sinusoids. In the machine, spatial independence of $(f^t)^{-1}(\cdot)$ is analogous, and the result is that the phase or direction of the flux linkage vector is the same as the direction of the current vector. The smooth air gap, and identical teeth result in $(f^t)^{-1}(\cdot)$ being independent of angle. Thus the magnitude of the output is independent of the phase angle of the input, and depends only on the input amplitude. Hence, the relation between flux and current can be written

$$\vec{\imath} = F(\vec{\lambda}) = f(\|\vec{\lambda}\|)\frac{\vec{\lambda}}{\|\vec{\lambda}\|} \tag{2}$$

where $f(\cdot)$ is the scalar function relating the magnitude of the input to the magnitude of the output. It has a similar shape to the inverse of the saturation function shown in Fig. 2, but is related to $f^t(\cdot)$ indirectly through (1). Note that one could consider the quantity $\|\vec{\lambda}\|/f(\|\vec{\lambda}\|)$ to be an inductance that varies as a function of $\|\vec{\lambda}\|$, so that $\vec{\imath} = \vec{\lambda}/L(\|\vec{\lambda}\|)$. This is the notation used in most discussions of the nonlinear T model, and is mathematically equivalent. We choose to use the $F(\cdot)$ notation instead, because it makes clear which terms are linear and which are not.

Now we are ready to model an entire machine with rotor and stator windings. Again, we consider an infinite number of infinitesimal teeth, but now we use complete tooth pairs, as represented by the electric and magnetic circuits in Figs. 3–7. The model for an infinitesimal angular element is as shown in Figs. 3–7. We can think of this model with an infinite number of teeth as a magnetic circuit, as shown in Fig. 4 or 5, but with each flux or MMF being an infinite-dimensional vector, over the spatial distribution of 2π rad, instead of just a scalar quantity.

The spatial distribution of the MMF between nodes A and B in Fig. 5 is forced by the sinusoidally distributed windings to be sinusoidal. However, the MMF distribution across each circuit element need not be exactly sinusoidal. Nevertheless, we will model the machine by assuming that the MMF across each element is in fact sinusoidal. There are several reasons that this can be expected to be a very good approximation. The rotor and stator saturation characteristics, $f_s^t(\cdot)$ and $f_r^t(\cdot)$, each have odd symmetry. If in addition, leakage inductance is low, and the rotor and stator saturation characteristics are similar to each other, the MMF at the center node in Fig. 5 will be, by symmetry, approximately the average of the rotor and stator MMF's. Thus it will be approximately sinusoidal.

TABLE I
REFERENCE FRAME SUPERSCRIPT DESIGNATIONS

superscript designation	reference frame	ρ
s	Stator	$\rho = 0$
r	Rotor	$\rho = \theta$
x	Arbitrary	ρ
e	Field-Oriented	$\angle(\vec{\lambda}_r^s)$

Furthermore, even if these conditions do not hold, and the MMF at the center node is not exactly sinusoidal, the effect of the harmonics on the result of interest, the fundamental component of the flux through the stator and rotor windings, will be small. This has been verified numerically [13].

Note that we are not assuming the flux distribution to be sinusoidal. However, since only the sinusoidal components of the flux distribution appear in the flux linkage, the flux linkage can be represented by a two-dimensional flux linkage vector. This results in an accurate lumped model for the dynamics of the machine as seen from terminal quantities, without explicitly including the flux distribution. The two nonlinear elements are modeled by functions of the form (2), which we call $F_s(\cdot)$ and $F_r(\cdot)$. These functions represent the saturation characteristics of the saturating portions of all the stator teeth or all the rotor teeth acting together, respectively. As before, the linear portions of the nonlinear inductances are lumped with the parallel inductances L_s and L_r, so that $F_s(\cdot)$ and $F_r(\cdot)$ include only second order and higher terms. For a machine with rotor and stator mechanically aligned, the model can be written

$$\vec{i}_s = F_s(\vec{\lambda}_s) + \left(\frac{1}{L_s} + \frac{1}{L_\ell}\right)\vec{\lambda}_s - \frac{1}{L_\ell}\vec{\lambda}_r \tag{3}$$

$$\vec{i}_r = F_r(\vec{\lambda}_r) + \left(\frac{1}{L_r} + \frac{1}{L_\ell}\right)\vec{\lambda}_r - \frac{1}{L_\ell}\vec{\lambda}_s \tag{4}$$

and

$$\dot{\vec{\lambda}}_s = \vec{v}_s - \boldsymbol{R}_s\vec{i}_s \tag{5}$$

$$\dot{\vec{\lambda}}_r = \vec{v}_r - \boldsymbol{R}_r\vec{i}_r \tag{6}$$

where the dot ($\dot{}$) indicates differentiation with respect to time. Due to the symmetry of the machine, the resistance matrices $\boldsymbol{R}_s$ and $\boldsymbol{R}_r$ are just the identity multiplied by scalar resistances. The subscript s or r on flux linkage or current (λ or i) indicates stator or rotor quantities. The superscript s indicates that the flux or current is measured in the stator, or stationary, reference frame, and the superscript r indicates coordinates fixed to the mechanical rotation of the rotor. Superscript designations of reference frames are summarized in Table I.

To account for the rotor being mechanically located at an angle θ, the rotor quantities are multiplied by $e^{\boldsymbol{J}\theta}$, where $\boldsymbol{J}$ is the elementary rotational matrix

$$\boldsymbol{J} = \begin{bmatrix} 0 & -1 \\ 1 & 0 \end{bmatrix}$$

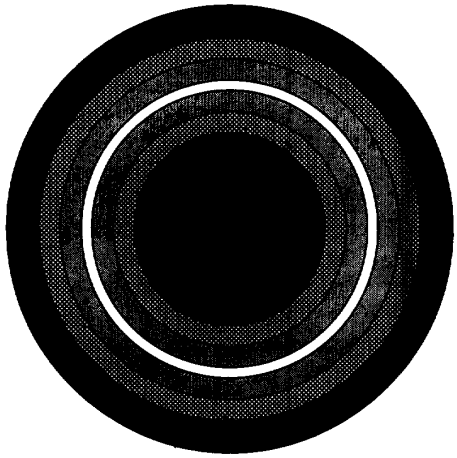

Fig. 8. Model for saturating induction machine using anisotropic materials.

to get

$$\vec{i}_s^s = F_s(\vec{\lambda}_s^s) + \left(\frac{1}{L_s} + \frac{1}{L_\ell}\right)\vec{\lambda}_s^s - \frac{1}{L_\ell}e^{\boldsymbol{J}\theta}\vec{\lambda}_r^r \tag{7}$$

$$e^{\boldsymbol{J}\theta}\vec{i}_r^r = F_r(e^{\boldsymbol{J}\theta}\vec{\lambda}_r^r) + \left(\frac{1}{L_r} + \frac{1}{L_\ell}\right)e^{\boldsymbol{J}\theta}\vec{\lambda}_r^r - \frac{1}{L_\ell}\vec{\lambda}_s^s. \tag{8}$$

Equation (8) can be multiplied by $e^{-\boldsymbol{J}\theta}$ to get

$$\vec{i}_r^r = F_r(\vec{\lambda}_r^r) + \left(\frac{1}{L_r} + \frac{1}{L_\ell}\right)\vec{\lambda}_r^r - \frac{1}{L_\ell}e^{-\boldsymbol{J}\theta}\vec{\lambda}_s^s \tag{9}$$

where we have taken advantage of the fact that the characteristics of the functions $F_s(\cdot)$ and $F_r(\cdot)$ allow moving a rotation ($e^{-\boldsymbol{J}\theta}$) inside or outside the function.

It is also possible to model the machine as being constructed of anisotropic materials, as shown in Fig. 8. The anisotropic materials are conceptual representations of the idealized behavior of a machine with an infinite number of teeth. This method has been used for modeling linear-motion induction machines with saturating magnetics [14]. The model in Fig. 8 is exactly equivalent to the magnetic circuit model discussed above, as the model for an infinitesimal angular element is the same.

IV. BLONDEL-PARK TRANSFORMATION

The characteristics of the functions $F_s(\cdot)$ and $F_r(\cdot)$ that allow moving a rotation ($e^{-\boldsymbol{J}\theta}$) inside or outside the function are useful because this allows performing the Blondel-Park transformation. We introduce the transformation

$$\begin{bmatrix} \vec{\lambda}_s^x \\ \vec{\lambda}_r^x \end{bmatrix} = T(\theta, \rho)\begin{bmatrix} \vec{\lambda}_s^s \\ \vec{\lambda}_r^r \end{bmatrix} \tag{10}$$

where

$$T(\theta,\rho)=\begin{bmatrix} e^{-\boldsymbol{J}\rho} & 0 \\ 0 & e^{\boldsymbol{J}(\theta-\rho)} \end{bmatrix} \tag{11}$$

and the superscript x indicates an arbitrary reference frame, at an angle ρ from the stator reference frame. Both θ and ρ may be time varying. The electrical dynamics become

$$\begin{bmatrix} \vec{\lambda}_s^x \\ \vec{\lambda}_r^x \end{bmatrix} = \begin{bmatrix} -\dot{\rho}\boldsymbol{J}\vec{\lambda}_s^x \\ (\dot{\theta}-\dot{\rho})\boldsymbol{J}\vec{\lambda}_r^x \end{bmatrix} + \begin{bmatrix} \vec{v}_s^x \\ \vec{v}_r^x \end{bmatrix} - \underline{\boldsymbol{R}}\left\{\underline{\boldsymbol{C}}_0\begin{bmatrix} \vec{\lambda}_s^x \\ \vec{\lambda}_r^x \end{bmatrix} + \begin{bmatrix} F_s(\vec{\lambda}_s^x) \\ F_r(\vec{\lambda}_r^x) \end{bmatrix}\right\} \tag{12}$$

where $\underline{\boldsymbol{C}}_0$ is defined by

$$\underline{\boldsymbol{C}}_0=\begin{bmatrix} \left(\frac{1}{L_s}+\frac{1}{L_\ell}\right)\boldsymbol{I} & -\frac{\boldsymbol{I}}{L_\ell} \\ -\frac{\boldsymbol{I}}{L_\ell} & \left(\frac{1}{L_r}+\frac{1}{L_\ell}\right)\boldsymbol{I} \end{bmatrix} \tag{13}$$

$$\begin{bmatrix} \vec{v}_s^x \\ \vec{v}_r^x \end{bmatrix} = T(\theta,\rho)\begin{bmatrix} \vec{v}_s^s \\ \vec{v}_r^r \end{bmatrix} \tag{14}$$

and $\underline{\boldsymbol{R}}$ is the 4 × 4 matrix of stator and rotor resistances. The principal benefit of the transformation is the removal of angular dependence from the dynamics (12), so that the system becomes time-invariant for constant speed $\dot{\theta}$. The transformation can be used to change to any reference frame, by the appropriate choice of ρ. One particularly useful choice of reference is the field-oriented reference frame. Aligning the reference frame with the rotor flux vector simplifies the model because the quadrature component of rotor flux is zero, and so the rotor flux vector can be treated as a scalar quantity. This can be used for field-oriented control techniques [9], [10].

We use different superscripts to designate the transformed quantities in different reference frames, summarized in Table I.

V. Torque Production

Since many common methods of calculating torque are valid only for linear magnetics, we must take care in calculating torque for the nonlinear-magnetics case. Because our model is flux-controlled, it is most straightforward to calculate the torque as a function of flux and angle by differentiating the field energy.[2]

$$\tau(\vec{\lambda}_s^s,\vec{\lambda}_r^r,\theta)=-\frac{\partial W_f(\vec{\lambda}_s^s,\vec{\lambda}_r^r,\theta)}{\partial\theta}. \tag{15}$$

We calculate W_f by $\int \vec{\boldsymbol{i}}^T d\vec{\boldsymbol{\lambda}}$.

$$\begin{aligned} W_f = &\int_0^{\lambda_{ra}} \left\{\left[F_r\left(\begin{bmatrix} x \\ 0 \end{bmatrix}\right)\right]^T + \left(\frac{1}{L_\ell}+\frac{1}{L_r}\right)[x \quad 0]\right\}\begin{bmatrix} dx \\ 0 \end{bmatrix} \\ &+\int_0^{\lambda_{rb}} \left\{\left[F_r\left(\begin{bmatrix} \lambda_{ra} \\ x \end{bmatrix}\right)\right]^T \right. \\ &\left. +\left(\frac{1}{L_\ell}+\frac{1}{L_r}\right)[\lambda_{ra} \quad x]\right\}\begin{bmatrix} 0 \\ dx \end{bmatrix} \\ &+\int_0^{\lambda_{sa}} \left\{\left[F_s\left(\begin{bmatrix} x \\ 0 \end{bmatrix}\right)\right]^T + \left(\frac{1}{L_\ell}+\frac{1}{L_s}\right)[x \quad 0]\right. \\ &\left. -\frac{1}{L_\ell}(e^{J\theta}\boldsymbol{\lambda}_r)^T\right\}\begin{bmatrix} dx \\ 0 \end{bmatrix} \\ &+\int_0^{\lambda_{sb}} \left\{\left[F_s\left(\begin{bmatrix} \lambda_{sa} \\ x \end{bmatrix}\right)\right]^T + \left(\frac{1}{L_\ell}+\frac{1}{L_s}\right)[\lambda_{sa} \quad x]\right. \\ &\left. -\frac{1}{L_\ell}(e^{J\theta}\boldsymbol{\lambda}_r)^T\right\}\begin{bmatrix} 0 \\ dx \end{bmatrix}. \end{aligned}$$

Fortunately, we can immediately drop all the θ-independent terms when computing torque. Thus, we use the expression

$$W_f=\left[-\frac{1}{L_\ell}e^{\boldsymbol{J}\theta}\vec{\lambda}_r^r\right]^T\vec{\lambda}_s^s+(\theta\text{ -independent terms}) \tag{16}$$

for the field energy. The torque is then

$$\tau(\vec{\lambda}_s^s,\vec{\lambda}_r^r,\theta)=\left[\frac{1}{L_\ell}\boldsymbol{J}e^{\boldsymbol{J}\theta}\vec{\lambda}_r^r\right]^T\vec{\lambda}_s^s \tag{17}$$

or in terms of the Park-transformed flux

$$\tau(\vec{\lambda}_s^x,\vec{\lambda}_r^x,\theta)=\left[\frac{1}{L_\ell}\boldsymbol{J}\vec{\lambda}_r^x\right]^T\vec{\lambda}_s^x=\frac{1}{L_\ell}(\lambda_{sq}^x\lambda_{rd}^x-\lambda_{sd}^x\lambda_{rq}^x). \tag{18}$$

This expression is identical to one form of the expression for the torque with linear magnetics. It can be shown to be equivalent to another common form, namely

$$\tau=\vec{i}_s^{xT}\boldsymbol{J}\vec{\lambda}_s^x. \tag{19}$$

VI. Verification of the Model and Determination of Machine Parameters

To verify the model, measurements were made on a 3-hp wound-rotor machine. The wound-rotor machine was a useful choice because it allowed access to rotor terminals, allowing more detailed verification of the model. In most practical applications, however, a squirrel-cage motor would be used, and measurement of rotor terminal quantities would be difficult if not impossible. For this reason, it is important to also verify that it is possible to find machine parameters, including saturation characteristics, with measurements only from the stator terminals. We first discuss measurements using the rotor terminals.

A. Doubly-Fed, Blocked Rotor Tests

The most straightforward way to test the magnetic model developed above is to block the rotor and characterize the magnetics using rotor and stator measurements. Ideally, the rotor should be blocked at $\theta = 0$. One could determine this position by applying a stator voltage and measuring open-circuit rotor voltage. Ideally, at $\theta = 0$ the rotor voltage is in phase with the stator voltage. However, stator resistance shifts this angle slightly. Another method is to put a rotor and a stator winding in series, and apply dc current. The torque thus generated will align the machine at $\theta = 0$. This was the method used.

With the rotor blocked at $\theta = 0$, the rotor and stator were fed from separate three-phase variable autotransformers. A set of 146 data points was taken on a grid of rotor and stator

[2] We use the convention that torque is positive in the motoring direction.

TABLE II
ERROR IN FIT OF π- AND T-MODELS TO MEASURED DATA

	T model fit to minimize voltage error	π model fit to minimize current error
Normalized current error, E_{norm}	0.192	0.082
Normalized voltage error, E_{norm}	0.088	0.103
Maximum rotor or stator current error at any data point	9.98 A	4.45 A

voltages, with the voltages in phase, up to about twice the rated voltage of the machine.

In order to fit the models to this data, it was necessary to use a parameterization of the scalar flux/current relationships, $f_s(\cdot)$ and $f_r(\cdot)$. We selected a function with the general shape of the saturation characteristic in Fig. 2, and with parameters that could be varied to get a good fit. The function used was

$$i = \frac{s_1 - s_2}{(b^{-n} + \lambda^{-n})^{1/n}} + s_2\lambda \tag{20}$$

where s_1 is the initial slope, s_2 is the final slope, b is the breakpoint, and n controls the sharpness of the transition between the two slopes. As n approaches infinity, the function approaches a piecewise linear function.

A numerical least-squares fit was performed to find the values of these parameters for the nonlinear inductors, and the values of the rotor and stator resistances. For the purposes of comparison, fits for the T model were also made. All inductors in both models were allowed to be nonlinear, so as to learn whether approximating the leakage inductance as linear is a good approximation. In order to make the numerical least-squares fit computationally efficient, it was necessary to use different error criteria for the two models. For the π model, parameters were computed to minimize error in the current predicted by the model, given each experimentally measured set of rotor and stator voltages. For the T model, the voltage error was minimized with the currents given. For the purpose of comparing the fit of the two models, errors were computed both ways for both models. The normalized error shown in Table II, E_{norm}, was computed by

$$E_{\text{norm}} = \sqrt{\frac{\sum_{i=1}^{N}(x_{i\,\text{meas}} - x_{i\,\text{model}})^2}{\sum_{i=1}^{N} x_{i\,\text{meas}}^2}} \tag{21}$$

where $x_{i\,\text{meas}}$ is the measured voltage or current, and $x_{i\,\text{model}}$ is the modeled voltage or current, at point i. Also listed is the maximum rotor or stator current error taken over all data points. Current error is likely to be more important, because in the state space equations, the model is used to calculate current from flux. From Table II, it appears that overall the π model has a better fit.

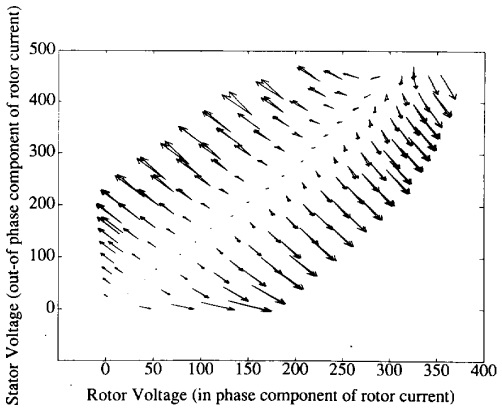

Fig. 9. π model rotor current vectors. Comparison of values predicted by the π model with measured data. Each data point consists of two vectors originating from the same point. The location of each origin indicates the rotor and stator rms line-to-line voltages, and the vectors indicate the calculated and measured rotor current vectors.

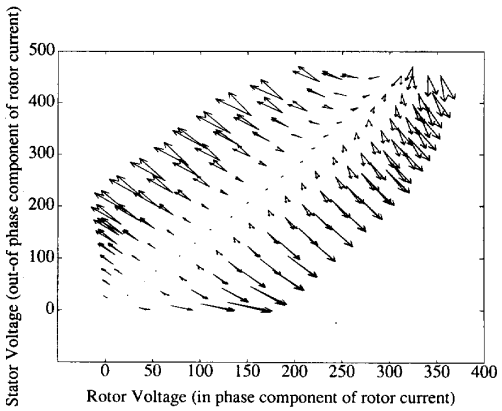

Fig. 10. T model rotor current vectors. Comparison of values predicted by the T model with measured data as in Fig. 9.

In Figs. 9 and 10, actual rotor currents are compared with rotor currents predicted for the π and T models. Current phasors are plotted originating from points representing the magnitude of the rotor and stator voltages. The measured and predicted current phasors in Fig. 9 correspond better than those in Fig. 10, showing that the π model better predicts the rotor current. Stator current phasor plots are similar, but rotor current is shown because effects of saturation are more apparent in the rotor. The rotor saturates at a lower flux level, because of its smaller cross-sectional area.

We conclude that, for this machine, both models fit well. The π model provides a slightly better fit when evaluated in terms of current error. We also note that the fit showed that leakage inductance in the π model is very close to linear. Leakage inductance in the T model is also close to linear, though this approximation may be less accurate. A fit using parallel resistance to model core loss was also carried out. Since this did not significantly improve the fit, it appears that core loss is in fact negligible, for the purpose of fitting an accurate model of machine dynamics in saturation.

B. Measurements Without Access to Rotor Terminals

The technique described above to measure the nonlinear characteristics of the machine is not directly useful for a squirrel cage machine, because it requires access to the rotor terminals. Thus, for most practical applications, a different method is necessary.

Synchronous speed or unloaded tests with higher-than-rated stator voltage are generally useful to drive the machine into saturation, and measure the flux-current characteristics. However, a series of synchronous speed tests at different voltages is insufficient to separately identify the rotor and stator saturation functions. At least one additional series of measurements must be performed with substantial slip in order to change the ratio of flux in the rotor and stator.

In order to verify that this procedure can yield parameters for a π model, a series of measurements were carried out on the same wound-rotor induction machine used for the measurements in Subsection A. Although the technique presented in this subsection is primarily intended for squirrel-cage machines, a comparison of the models derived from the two different measurement techniques is useful to verify both the two methods and the model. Since the first method requires a wound rotor machine, both sets of measurements were performed on the same machine to allow comparison between the results of the two methods.

The stator was driven at 60 Hz from a 220-V three-phase variac, followed by a a step-up transformer to allow up to twice rated voltage to be applied to the machine. Voltage and current into the stator were measured and analyzed, and the results recorded by a digital power meter.

The machine was connected to a 40-kW separately excited dynamometer, with digital strain-gauge torque measurement. A 1024-count incremental optical shaft encoder was connected to a frequency counter to read rotation frequency. Because of mechanical vibration in the system, digital torque readings were noisy and unreliable. The addition of a low-pass filter to the torque signal solved this problem. Friction in the outer bearings of the dynamometer was measured by operating the dynamometer as a motor and reading the torque scale. This measurement was added to the torque readings in normal operation.

Data were recorded for a series of voltages ranging from just below rated voltage to just below twice rated voltage. At each voltage, the system was operated with a series of successively larger loads, in increments of approximately 2/3 rated load. Voltage was only approximately constant as the load was varied, and all data was recorded for each torque/voltage combination.

Parameters for the model were found using a numerical least-squares fit, similar to those used in Subsection A. The measurements were compared to the model's predictions for the same mechanical speed and stator voltage. A minimum in the weighted sum of squared error of current magnitude, torque, and power input was approximated by the numerical minimization program. The weightings given to current and torque were approximately equal relative to full-scale measurements of those quantities, but power was given a lower weighting (one quarter) because the model does not attempt to accurately model core losses. The fit determined four parameters each for rotor and stator saturation curves, and used a linear leakage inductance. The minimization was performed both using measured dc rotor and stator resistances, and with these resistances as free parameters. In practice, at least the rotor resistance would need to be a free parameter in the measurement of a squirrel-cage machine.

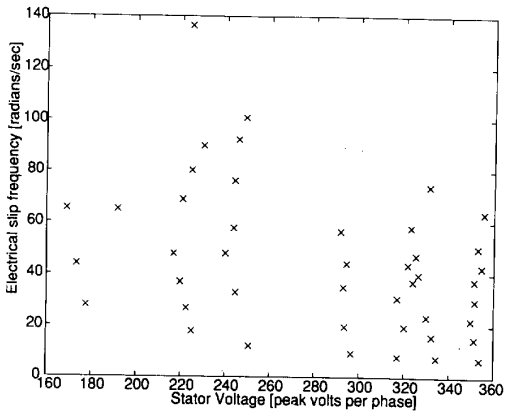

Fig. 11. Locus of measured data.

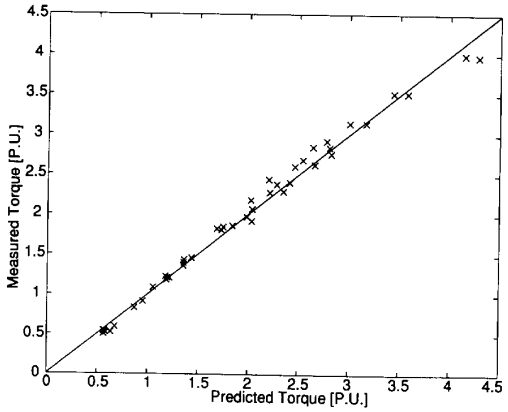

Fig. 12. Comparison of measured and modeled torque. Model fit two nonlinear inductances and linear leakage inductance using shorted-rotor measurements.

Fig. 11 shows the locus of the data on the voltage-slip plane. Figs. 12–17 compare measured variables to those predicted by the model. In Figs. 12–14, the parameters for the model are those estimated as discussed above, with resistances measured at dc. Figs. 15–17 use all parameters, including resistance, as estimated by the numerical fit. Although rotor resistance as estimated by the fit was very close to the dc value, stator resistance was estimated at nearly twice the dc value. It is not clear to what extent this increased stator resistance is a result of higher ac resistance in the stator windings, and to what extent it models core losses, but in any case, the fit to the power curve is markedly better with the higher stator resistance. It is notable that torques up to four times rated torque were achieved, and modeled with reasonable accuracy.

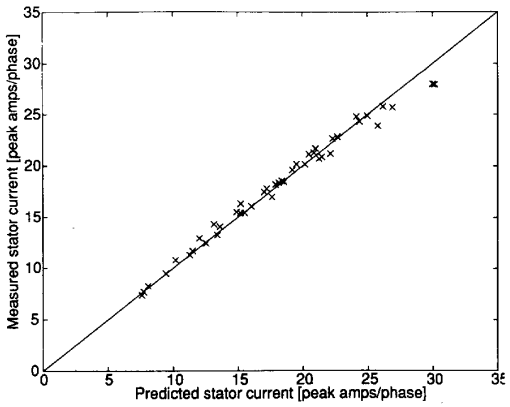

Fig. 13. Comparison of measured and modeled current. Model fit two nonlinear inductances and linear leakage inductance using shorted-rotor measurements.

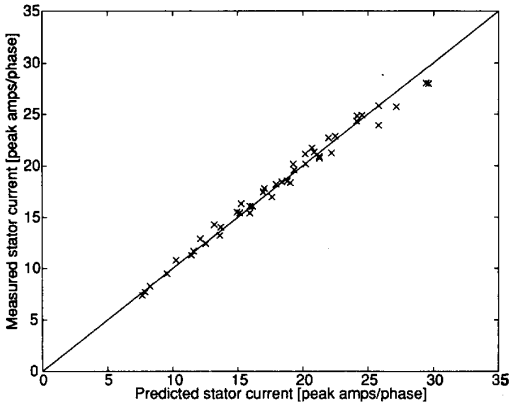

Fig. 16. Comparison of measured and modeled current. Model fit two nonlinear inductances, linear leakage inductance, and two resistances using shorted-rotor measurements.

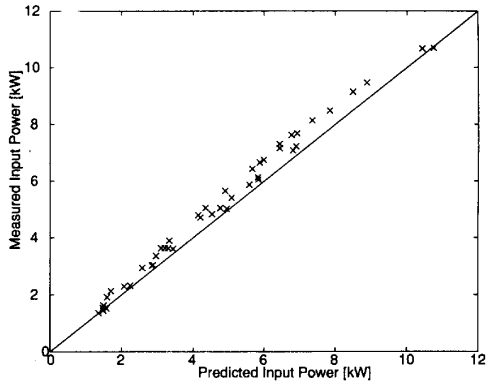

Fig. 14. Comparison of measured and modeled power. Model fit two nonlinear inductances and linear leakage inductance using shorted-rotor measurements.

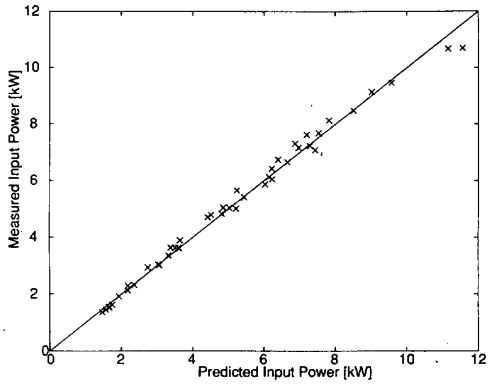

Fig. 17. Comparison of measured and modeled power. Model fit two nonlinear inductances, linear leakage inductance, and two resistances using shorted-rotor measurements.

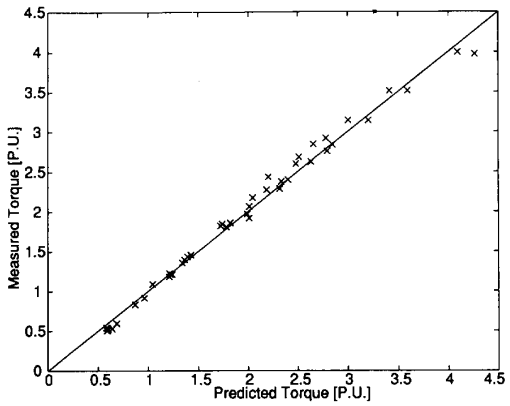

Fig. 15. Comparison of measured and modeled torque. Model fit two nonlinear inductances, linear leakage inductance, and two resistances using shorted-rotor measurements.

Figs. 18 and 19 compare the stator and rotor curves as determined using the measurements of Subsection A to those determined as discussed above. All the curves shown were determined by fits including rotor and stator resistances as free parameters, and constraining leakage inductance to be linear. It is apparent that the parameterization determined by either method is very similar.

VII. Steady-State Operation in Saturation

One interesting implication of the π model is that, unlike transformers, smooth air-gap machines with balanced sinusoidal voltage excitation and sinusoidally distributed windings have sinusoidal terminal currents even in heavy saturation. In a transformer, the magnitude of the flux changes at the supply frequency, going from saturation in one direction through zero to saturation in the other direction and back. But in the smooth air-gap machine, the flux vector stays at a constant magnitude, and rotates at the supply frequency, and so the current vector does likewise. This constant-magnitude rotating current vector corresponds to sinusoidal phase currents. The model can also be used to show that the waveforms in saturation do not remain sinusoidal with unbalanced sinusoidal excitation.

We now consider operation with the rotor shorted, corresponding to a squirrel-cage machine. In steady-state operation,

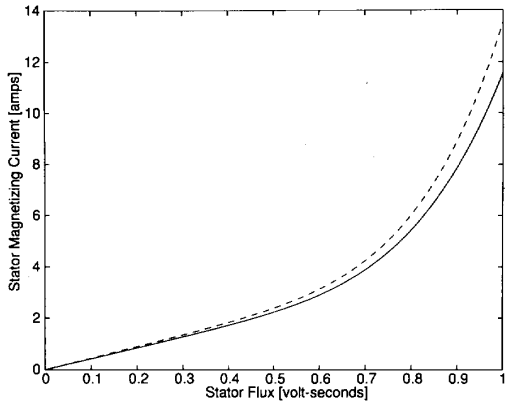

Fig. 18. Stator saturation characteristics. Solid: Fit to measurements in Subsection A. Dashed: Fit to shorted-rotor torque tests described in Subsection B.

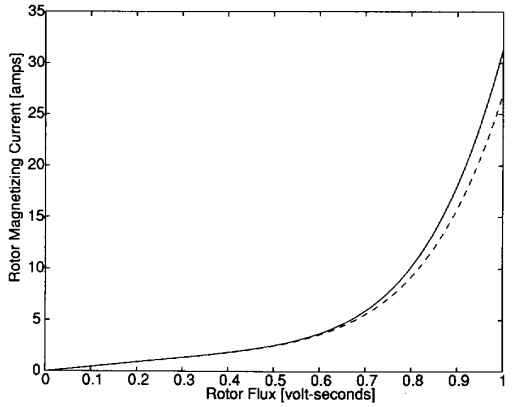

Fig. 19. Rotor saturation characteristics. Solid: Fit to measurements in Subsection A. Dashed: Fit to shorted-rotor torque tests described in Subsection B.

with a fixed mechanical speed and torque, there is one degree of freedom that may be adjusted to optimize the efficiency. This is often discussed in terms of finding the optimal slip, but finding the optimal rotor flux is equivalent. Assuming all loss is copper loss, the rotor flux for operation at a given torque with minimal loss is independent of the speed or frequency. For this reason, we approach optimal efficiency operation in terms of finding the optimal rotor flux. Our result is only correct if core loss is negligible. Although core loss often may be neglected in calculating dynamics for such applications as control design, it is more important for efficiency calculations. Nonetheless, the analysis without core loss can be useful in understanding general trends in how a machine performs when driven far into magnetic saturation, and in identifying useful ranges of operation for particular applications.

From a given torque and rotor flux we calculate loss, using the rotor-flux oriented reference frame. From the equations of motion in this frame [9]

$$\dot{\rho} = \frac{R_r}{L_\ell}\frac{\lambda^e_{sq}}{\lambda^e_{rd}} + \dot{\theta}. \tag{22}$$

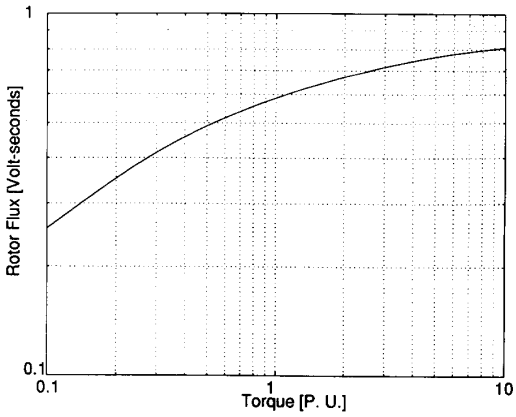

Fig. 20. Rotor flux for optimal efficiency operation.

$$\dot{\lambda}^e_{rd} = -R_r\left[\left(\frac{1}{L_r}+\frac{1}{L_\ell}\right)\lambda^e_{rd} - \frac{1}{L_\ell}\lambda^e_{sd} + f_r(\lambda^e_{rd})\right] \tag{23}$$

$$\dot{\vec{\lambda}}^e_s = -\dot{\rho}\boldsymbol{J}\vec{\lambda}^e_s + \vec{v}^e_s - R_s\left\{\left(\frac{1}{L_s}+\frac{1}{L_\ell}\right)\vec{\lambda}^e_s - \frac{1}{L_\ell}\begin{bmatrix}\lambda^e_{rd}\\0\end{bmatrix} + F_s(\vec{\lambda}^e_s)\right\} \tag{24}$$

we find the stator flux

$$\lambda^e_{sd} = L_\ell\left[\left(\frac{1}{L_r}+\frac{1}{L_\ell}\right)\lambda^e_{rd} + f_r(\lambda^e_{rd})\right] \tag{25}$$

and

$$\lambda^e_{sq} = -\tau\frac{L_\ell}{\lambda^e_{rd}}. \tag{26}$$

The stator current is then

$$\vec{i}^e_s = F_s(\vec{\lambda}^e_s) + \left(\frac{1}{L_s}+\frac{1}{L_\ell}\right)\vec{\lambda}^e_s - \frac{1}{L_\ell}\begin{bmatrix}\lambda^e_{rd}\\0\end{bmatrix} \tag{27}$$

and similarly the rotor current is

$$\vec{i}^e_r = \begin{bmatrix} f_r(\lambda^e_{rd}) + \left(\frac{1}{L_r}+\frac{1}{L_\ell}\right)\lambda^e_{rd} \\ 0 \end{bmatrix} - \frac{1}{L_\ell}\vec{\lambda}^e_s \tag{28}$$

where $f_r(\cdot)$ is the scalar version of $F_r(\cdot)$. The loss is

$$P_{\text{loss}} = \|i_s\|^2 R_s + \|i_r\|^2 R_r. \tag{29}$$

The rotor flux giving a minimum loss at torque τ can then be found numerically.

This optimal rotor flux has been calculated for the experimentally measured machine in Section VI. Torque was calculated from the model as discussed in Section V. The calculated optimal rotor flux is shown as a function of the torque in Fig. 20. Figs. 21–25 show other calculated parameters as a function of torque. While Figs. 20 and 21 are valid for any speed, for Figs. 22–25 the machine's rated speed of 1800 r/min was assumed. The figures show torque up to ten times the machine's rating. However, the validity of the model has only been tested up to four times rated torque for this machine. Thus, beyond four times rated torque, the curves are only extrapolations, meant to be illustrative of general trends, not representations of experimental results.

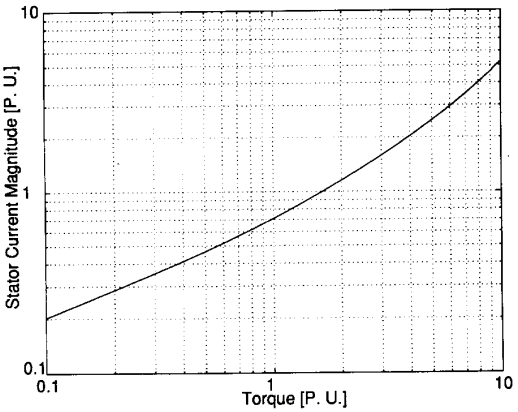

Fig. 21. Stator current for optimal efficiency operation.

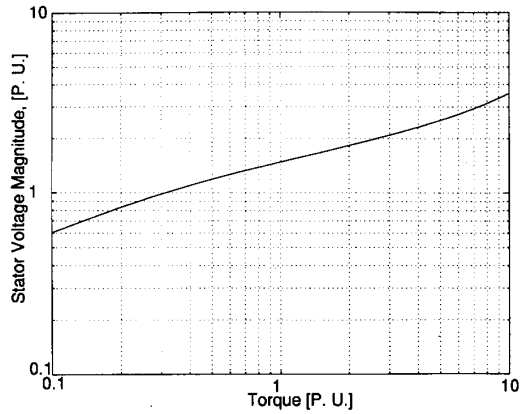

Fig. 22. Stator voltage for optimal efficiency operation.

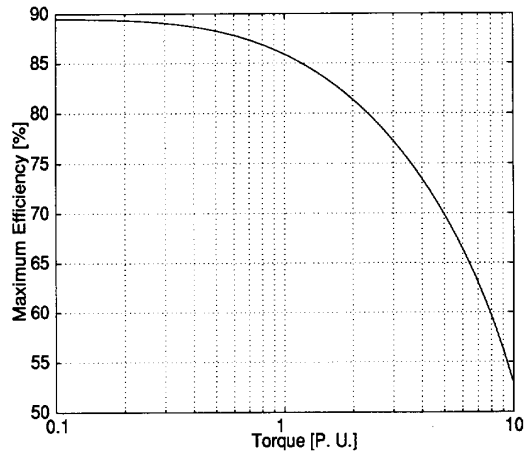

Fig. 23. Maximum efficiency as a function of torque.

From these figures, we can see that at ten times rated full load torque, efficiency has dropped to 53%. This is significantly lower than the efficiency between zero and rated torque, 89%, but is still usable in some situations. The current required increases rapidly above rated torque, with five times rated current required for ten times rated torque. Voltage, however, does not increase as quickly. In fact, the voltage required is lower than would be expected if the machine remained linear at high flux levels. Less than four times rated voltage is needed for ten times rated torque. Furthermore, if the increased torque is required only at lower speeds, the voltage required would be even lower. Power output per V-A input decreases at high torques, due to decreases in both efficiency and power factor. While the curves shown here are specific to one machine, they give a general idea of the possibilities for operation of any induction machine at torque levels well above its rating, and could be recalculated for any particular machine.

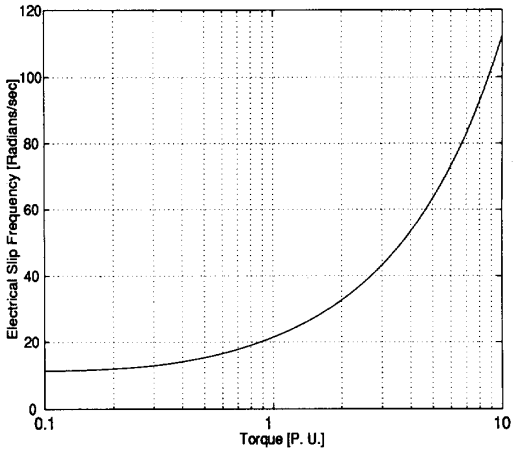

Fig. 24. Slip for optimal efficiency operation.

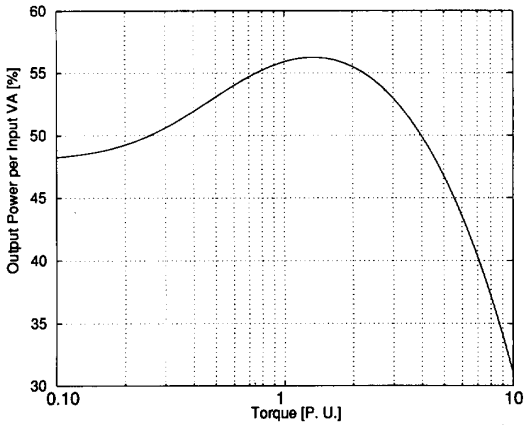

Fig. 25. Output power per input V-A in optimal efficiency operation.

VIII. Field-Oriented Control

Field-oriented control decouples the control of rotor flux and torque in the linear-magnetics case. However, cross-saturation effects can severely disrupt performance of a control system designed without taking these effects into account [15]. Although control systems based on the T model and the use of a current source inverter have been developed to

mitigate these problems [6], [16]–[18], the resulting designs are somewhat awkward. In contrast, with the flux-controlled π model, by using the stator flux as an intermediate control variable, it is possible to obtain a simple decoupled control of rotor flux and torque [9]. An experimental implementation of this control resulted in significant performance improvements compared to a simple field-oriented control scheme based on linear magnetics [10].

IX. Conclusion

A new nonlinear π model of induction machines operating in magnetic saturation has been developed. It is based on a magnetic circuit model of a rotor-stator tooth pair, with two nonlinear reluctance elements representing the saturation in the rotor and in the stator. The model of a tooth pair is extended to a model of the machine by assuming an infinite number of infinitesimal teeth. The model is compatible with the Blondel-Park transformation, and so, many standard analysis and control methods can be applied. Comparisons with measured data show a slightly better fit for the new nonlinear π model than for the nonlinear T model. The π model's predictions of torque up to four times the rated torque of the machine were experimentally verified. The π model is preferred to the T model because it is more closely based on a physical model of the machine, and because it can be easier to use in simulation and control. Operation with minimal resistive losses has been analyzed as an approximation to optimal efficiency operation in the case that hysteresis and eddy current losses in the iron are small.

References

[1] J. E. Brown, K. P. Kovacs, and P. Vas, "A method of including the effects of main flux path saturation in the generalized equations of a.c. machines," *IEEE Trans. Power App. and Syst.*, vol. PAS-102, no. 1, pp. 96–103, Jan. 1983.

[2] P. Vas, K. E. Hallenious, and J. E. Brown, "Cross-saturation in smooth-air-gap electrical machines," *IEEE Trans. Energy Conversion*, vol. EC-1, no. 1, pp. 103–109, Mar. 1986.

[3] R. J. Kerkman, "Steady-state and transient analysis of an induction machine with saturation of the magnetizing branch," *IEEE Trans. Ind. Applicat.*, vol. IA-21, no. 1, pp. 226–234, Jan./Feb. 1985.

[4] J. Robert, "A simplified method for the study of saturation in ac machines," in *Modelling and Simulation of Electrical Machines and Power Systems*, J. Robert and D. K. Tran, Eds. North Holland: Elsevier Science Publishers B. V., 1988, pp. 129–136.

[5] M. S. Garrido, L. Pierrat, and E. Dejaeger, "The matrix analysis of saturated electrical machines," in *Modelling and Simulation of Electrical Machines and Power Systems*, J. Robert and D. K. Tran, Eds. North Holland: Elsevier Science Publishers B. V., 1988, pp. 137–144.

[6] P. Vas, *Vector Control of AC Machines*. Oxford University Press, 1990.

[7] R. D. Lorenz and D. W. Novotny, "Saturation effects in field-oriented induction machines," *IEEE Trans. Ind. Applicat.*, vol. 26, no. 2, pp. 283–289, Mar./Apr. 1990.

[8] F. M. H. Khater, R. D. Lorenz, D. W. Novotny, and K. Tang, "Saturation effects in field-oriented induction machines," *IEEE Trans. Ind. Applicat.*, vol. IA-23, no. 2, pp. 276–282, Mar./Apr. 1987.

[9] C. R. Sullivan and S. R. Sanders, "Modeling the effects of magnetic saturation on electrical machine control systems," in *Nonlinear Contr. Syst. Design 1992*, selected papers from the 2nd IFAC Symp., 1992, pp. 69–76.

[10] C. Kao, C. R. Sullivan, B. Acker, and S. R. Sanders, "Induction machine control systems with magnetic saturation," in *PESC '94 Rec. 25st Annu. IEEE Power Electron. Specialists Conf.*, 1994, pp. 250–258.

[11] X. Z. Liu, G. C. Verghese, and J. H. Lang, "Generalizing the Blondel-Park transformation of electrical machines: Necessary and sufficiennt conditions," *IEEE Trans. Circuits and Syst.*, vol. 36, no. 8, pp. 1058–1067, Aug. 1989.

[12] M. Vidyasagar, *Nonlinear System Analysis*. Englewood Cliffs, NJ: Prentice-Hall, 1978, pp. 97–112, ch. 4.1.

[13] C. R. Sullivan and S. R. Sanders, "Models for induction machines with magnetic saturation of the main flux path," in *Conf. Rec. IEEE Ind. Applicat. Soc. Annu. Meeting*, 1992, vol. 1, pp. 123–131.

[14] K. Idir, G. E. Dawson, and A. R. Eastham, "Modeling and performance of linear induction motor with saturable primary," *IEEE Trans. Ind. Applicat.*, vol. 29, no. 6, pp. 1123–1128, Nov./Dec. 1993.

[15] P. Vas and M. Alakula, "Field-oriented control of saturated induction machines," *IEEE Trans. Energy Conversion*, vol. 5, no. 1, pp. 218–223, Mar. 1990.

[16] E. Levi, S. Vukosavic, and V. Vuckovic, "Saturation compensation schemes for vector controlled induction motor drives," in *PESC '90 Rec.*, 1990, pp. 591–598.

[17] E. Levi and V. Vuckovic, "Field-oriented control of induction machines in the presence of magnetic saturation," *Electric Machines and Power Syst.*, vol. 16, no. 2, pp. 133–147, 1989.

[18] Z. Krzeminski, "Differential equations of induction motor with nonlinear control synthesis with regard to saturation of main magnetic path," *Rozprawy Elektrotechniczne*, vol. 34, no. 1, pp. 117–131, 1988.

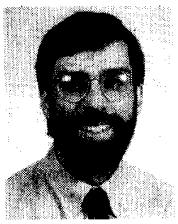

Charles R. Sullivan (S'92) was born in Princeton, NJ, in 1964. He received the B.S. degree in electrical engineering with highest honors from Princeton University in 1987.

Between 1987 and 1990, he worked at Lutron Electronics, Coopersburg, PA, developing high-frequency dimming ballasts for compact fluorescent lamps. He is currently a Ph.D. candidate in electrical engineering at the University of California, Berkeley. He has published technical papers on numerous topics including thin-film magnetics for high-frequency power conversion, dc–dc converter topologies, energy and environmental issues, and modelling, analysis, and control of electric machines.

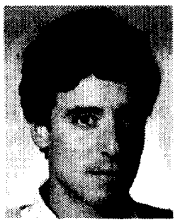

Seth R. Sanders (S'88–M'88) received the S.B. degree in electrical engineering and physics, and the S.M. and Ph.D. degrees in electrical engineering from Massachusetts Institute of Technology, Cambridge, MA, in 1981, 1985, and 1989, respectively.

He worked as a design engineer at the Honeywell Test Instruments Division, Denver, CO from 1981 to 1983. He is presently Assistant Professor in the Department of Electrical Engineering and Computer Sciences, University of California, Berkeley. His research interests are in power electronics, variable speed drive systems, simulation, and in nonlinear circuit and system theory as related to the power electronics field. During the 1992–93 academic year, he was on industrial leave with National Semiconductor, Santa Clara, CA.

Dr. Sanders is a recipient of the NSF Young Investigator Award in 1993. He serves as Chair of the IEEE Technical Committee on Computers in Power Electronics.